On the Temperature Sensitivity of 1.5-μm GaInNAsSb Lasers

Seth R. Bank, *Student Member, IEEE*, Lynford L. Goddard, *Student Member, IEEE*, Mark A. Wistey, *Student Member, IEEE*, Homan B. Yuen, *Student Member, IEEE*, and James S. Harris, Jr., *Fellow, IEEE*

***Abstract*—We analyze the temperature sensitivity of 1.5-μm GaInNAsSb lasers grown on GaAs. Building on the method of Tansu and coworkers, we find evidence that the characteristic temperatures for the threshold current T_0 and external efficiency T_1 are balanced by a combination of monomolecular recombination and temperature destabilizing mechanism(s) near room temperature. At elevated temperatures, the destabilizing process(es) dominate, due to increased threshold current density $J_{\rm th}$. While it is difficult to definitively identify carrier leakage, Auger recombination, or a combination of the two as the responsible mechanism(s), results indicate that carrier leakage certainly plays a role. Evidence of intervalence band absorption was also found; T_1 was reduced, but $J_{\rm th}$ and T_0 were not significantly degraded. Conclusions are corroborated by supporting measurements of the Z-parameter with bias, spontaneous emission spectrum, and band-offsets. Spontaneous emission measurements show evidence of weak Fermi-level pinning within the active region at threshold, indicating a form of carrier leakage. This is consistent with the characteristic temperature analysis and a leakage mechanism is proposed. This process is partially responsible for the greater temperature sensitivity of device parameters and the poor internal efficiency. Methods for reducing the effects of each parasitic mechanism are also described.**

***Index Terms*—Auger recombination, carrier leakage, GaInNAs, GaInNAsSb, gallium arsenide, intervalence band absorption, semiconductor laser.**

I. Introduction

DILUTE nitride lasers, grown on GaAs, have received considerable attention in recent years due to their potential to cover the entire 1.2 to 1.6 μm range for optical fiber communication [1]–[6]. While the possibility of integration with Al(Ga)As–GaAs distributed Bragg reflectors is an important advantage for monolithic vertical-cavity surface-emitting laser (VCSEL) sources, a fundamental advantage of GaInNAs and GaInNAsSb lies in the large conduction band offsets. The relatively small conduction band offsets of InGaAsP alloys cause electron leakage that compounds Auger recombination and limits T_0 [7]. While T_0 values approaching 100 K have been observed in buried heterostructure devices with strained multiple quantum well (QW) active regions [8], characteristic temperatures $\sim$60–80 K are more typical literature values for InGaAsP. These observations are consistent with theoretical calculations that show lasers dominated by Auger recombination must have $T_0 \leq T/3 \approx 100$ K at room temperature [9].

By contrast, it was predicted theoretically [10] and found experimentally [11], [12] that the reduction in bandgap due to the addition of nitrogen into GaAs, takes place primarily in the conduction band. As a result, it has been speculated that GaInNAs lasers should not suffer from similar electron leakage effects [13]. Moreover, as will be shown, the bandgap discontinuities at the separate confinement heterostructure interface for AlGaAs–GaAs are sufficient to suppress diffusive leakage [14]. Drift leakage is also quite small due to the relatively high conductivity of even moderately doped ($\gtrsim 1\times10^{17}$ cm^{-3}) AlGaAs cladding layers. This has been borne out by experiment and GaInNAs lasers show excellent temperature stability with $T_0 > 100$ K being quite common [15]. Care must be exercised, however, as large values of T_0 may be obtained if the threshold current is dominated by monomolecular recombination due to its weak temperature dependence [16], [17]. Application of the Tansu analysis to 1.3-μm GaInNAs lasers with low monomolecular recombination showed evidence of a temperature destabilizing mechanism that was identified as hole leakage [18], [19]. Evidence of Auger recombination has also been found in high-quality 1.3-μm GaInNAs lasers using the Z-parameter technique [20] and it is expected that such effects should increase at 1.5 μm due to the smaller quantum well (QW) bandgap [21]. However, it is difficult to determine the exact mechanism as neither the Tansu analysis nor the Z-parameter technique can sufficiently discriminate between carrier leakage and Auger recombination. Hydrostatic pressure measurements are promising as they are capable of differentiating between carrier leakage and Auger recombination, but the pressure dependence of radiative recombination complicates interpretation [22]. Additionally, the exact leakage path remains an open question; injected carriers may escape the QW, but must recombine outside the active region to be truly lost as leakage. Regardless of the physical mechanism(s), the inherent temperature sensitivity of the alloy is of great interest as it will likely determine the commercial viability of dilute nitride active layers for inexpensive uncooled telecommunication and high-power pump laser sources. It is also of great importance to determine the root cause(s) of the temperature sensitivity of 1.5-μm GaInNAsSb lasers to provide insight for further improvement. The analysis presented here investigates the various physical mechanisms at work that serve to increase the temperature sensitivity and cause the low efficiencies that have been reported [4]–[6], [23].

Manuscript received December 3, 2004; revised June 20, 2005. This work was supported by the Army Research Office and Defense Advanced Research Projects Agency under Grants DAAD17-02-C-0101 and MDA972-00-1-024, and also by Stanford Network Research Center (SNRC). The work of L. L. Goddard was supported by a National Physical Science Consortium Fellowship and stipend support from Xerox Palo Alto Research Center.

The authors are with the Solid State and Photonics Laboratory, Stanford University, Stanford, CA 94305 USA (e-mail: sbank@stanfordalumni.org).

Digital Object Identifier 10.1109/JSTQE.2005.853852

This paper is divided into five sections. In Section II, the method of Tansu and coworkers [17] for characterizing laser performance as a function of both cavity length and ambient temperature is reviewed. Section III discusses the devices used in the analysis and the results obtained. It is found that the temperature stability is degraded in comparison to 1.3-μm lasers, due to increased carrier leakage and to some degree, intervalence band absorption (IVBA). Strong evidence of carrier leakage is found in the highly temperature dependent internal efficiency and the peak gain coefficient, consistent with the degradation of GaInNAs lasers as the wavelength is extended beyond 1.3 μm [24]. In Section IV, several ancillary measurements are presented to corroborate many of the conclusions. Bias dependent spontaneous emission spectra show significant carrier leakage effects. It is observed that emission from higher levels within the QW and barriers pin only weakly at threshold. Additionally, Z-parameter measurements show significant monomolecular recombination at low current densities and a temperature destabilizing mechanism at high bias, in agreement with the findings of the Tansu analysis. It is expected that non-radiative recombination can be minimized through further improvements in growth technology, similar to the steady improvement of GaInNAs lasers at 1.3 μm [25], but leakage and Auger recombination are more difficult obstacles. Thermionic escape times were also calculated from the known band offsets and are found to be significantly shorter than the radiative lifetime. The conclusions are summarized in Section V and methods for reducing the severity of each effect are discussed. A possible leakage mechanism is also identified.

II. Variation of Cavity Length and Temperature

This section describes the method of Tansu and coworkers for characterizing the temperature dependence of lasers. First applied to InGaAs lasers emitting $\sim$1.2 μm [17], it has also been used to characterize GaInNAs lasers at 1.3 μm [18], [26]. Typical cavity length studies consist of measuring the threshold current density $J_{\rm th}$ and the external differential quantum efficiency η_e with cavity length to obtain the important device parameters at room temperature. Through variation of both cavity length L and temperature T, a characteristic temperature is measured for each device parameter: $J_{\rm th}, \eta_e, J_{\rm tr}$ (transparency current density), η_i (internal quantum efficiency), $\alpha_{\rm i}$ (internal loss) and g_0 (peak gain coefficient). In conjunction with other techniques such as spontaneous emission [27] and Z-parameter [7] measurements, a fuller understanding of the relevant physics is obtained.

The laser gain balances the loss at threshold and $J_{\rm th}$ may be written as [28]

$$J_{\rm th} = \frac{J_{\rm tr}}{\eta_i} \cdot \exp\left(\frac{\alpha_i + \alpha_m}{\Gamma \cdot g_0}\right) \approx \frac{J_{\rm tr}}{\eta_{i,\,\rm above,\,th}} \cdot \exp\left(\frac{\alpha_i + \alpha_m}{\Gamma \cdot g_0}\right) \tag{1}$$

under the assumption of a logarithmic gain-current relation. Here, η_i is the (below threshold) internal quantum efficiency, α_m is the mirror loss, and Γ is the 2-D overlap between the optical mode and the QW.

Above threshold, η_e is proportional to η_i [29]

$$\eta_e = \eta_i \cdot \frac{\alpha_m}{\alpha_i + \alpha_m}. \tag{2}$$

In (2), η_i is the *above threshold* internal efficiency which is typically assumed to be the same as the below threshold value. The internal quantum efficiency is further defined as the fraction of input current that generates light-emitting carriers in the active layer [30] and may be written as [27]

$$\eta_i = \eta_{\rm spread} \cdot \eta_{\rm rad} \cdot \eta_{\rm inj}. \tag{3}$$

The effect of lateral current spreading is usually assumed to be negligible, $\eta_{\rm spread} \approx 1$. Current spreading may be neglected if the stripe width is much greater than the carrier diffusion length. Broad-area 20-μm-wide ridge-waveguide lasers were used in this study and near room temperature, $\eta_{\rm spread} = 0.84$ was found [31] using the method of [27]. The error incurred by this assumption overestimates $J_{\rm tr}$ by $<20\%$ but has no effect on its characteristic temperature or any other device parameters. A second assumption is that the carrier density clamps *within the active layer* at threshold and the differential radiative efficiency $\eta_{\rm rad}$ should be close to unity [27]. The value of η_i then approaches the injection efficiency $\eta_{\rm inj}$. As we shall see in Section IV, the carrier density clamps softly at threshold and it is not valid to assume $\eta_i \rightarrow \eta_{\rm inj}$. A third assumption that must be made is that η_i is the same above and below threshold. This simplification is implicit in cavity length studies [17] and is shown explicitly with the approximate relationship in (1). This is somewhat dubious in the presence of large non-radiative recombination, but is necessary to calculate g_0 and $J_{\rm tr}$ and only affects the value of $J_{\rm tr}$. Inaccuracy of this assumption manifests itself as an increase in the calculated $J_{\rm tr}$, in proportion to the ratio of the above and below threshold values of η_i. All other parameters are unaffected. Measurement of both $J_{\rm th}(L,T)$ and $\eta_e(L,T)$ then allows the extraction of all the relevant device parameters and their characteristic temperatures.

By taking the derivative of (1) and (2) with respect to temperature, T_0 and T_1 may be decomposed into the contributions of each device parameter [17]

$$\frac{1}{T_0} = \frac{1}{T_{\rm tr}} + \frac{1}{T_{\eta_i}} + \frac{\alpha_i + \alpha_m}{\Gamma \cdot g_0}\frac{1}{T_{g_0}} + \frac{\alpha_i}{\Gamma \cdot g_0}\frac{1}{T_{\alpha_i}} \tag{4}$$

and

$$\frac{1}{T_1} = \frac{1}{T_{\eta_i}} + \frac{\alpha_i}{\alpha_i + \alpha_m}\frac{1}{T_{\alpha_i}} \tag{5}$$

assuming each parameter x may be fitted to an Arrhenius relation $T_x^{-1} = \pm x^{-1}{\rm d}x/{\rm d}T$. The terms $T_{\rm tr}, T_{\eta i}, T_{g_0}$, and $T_{\alpha i}$ are the characteristic temperatures for $J_{\rm tr}, \eta_i, g_0$, and α_i, respectively.

III. Experiment Results

A. Sample Preparation and Measurement

The devices used in this study were edge-emitting broad-area separate confinement heterostructure ridge-waveguide lasers, grown on GaAs by molecular beam epitaxy. Lasing occurred in the range 1.46–1.51 μm, depending upon location on the wafer

and operating temperature. Room temperature $J_{\rm th}$ was $\sim$1–1.3 kA/cm^2 and T_0 was in the range 85–105 K for long cavity devices. Details of the growth and fabrication are described elsewhere [6], [23]. A highly reflective (HR) coating was applied to one facet and the other was left as-cleaved.

Lasers were mounted on a temperature controlled copper chuck and measured under low duty cycle pulsed conditions (1 μs, 1% duty cycle) from 15 °C to 75 °C in 5 °C steps. Care was taken to ensure maximal Fermi level pinning in the QW by extracting the threshold and efficiency from output powers in the range of 5–12 mW [32], [33]. This corresponds to a range of $J/J_{\rm th} \approx 1.2$–1.4 times above threshold at 15 °C. At 75 °C, the ratio was reduced slightly 1.1–1.25 times threshold. This may cause a slight reduction in the measured α_i and an increase in η_i at elevated temperature [33]. To avoid the lasing "knee" and heating effects, data points were rejected if the linearity of the light output with current input (L–I) had a coefficient of determination $R^2 < 0.998$. Most measurements showed $R^2 > 0.999$, but degradation of R^2 was observed at elevated temperatures. No concavity was observed in the L-I curves over the 5–12 mW range at any temperature. To reduce the propagation of measurement error, each $J_{\rm th}(T)$ and $\eta_e(T)$ were fitted to local Arrhenius relations. The fitted data were used in the cavity length calculations to extract the device parameters and their characteristic temperatures. Measurement over a wide temperature range is required to obtain accurate characteristic temperatures. While the 60 K range employed here is not sufficient to precisely quantify the temperature sensitivity of weakly varying parameters, the values determined here serve to gauge their relative temperature dependence and to compare with other reports.

Several long cavity devices with two fixed cavity lengths were used to determine device parameters, to avoid the short cavity effects observed in Section III-B. This also reduced the interpretation complexity caused by the bias dependent nature of the temperature sensitivity for different cavity lengths. As will be shown later, the turn-on of the temperature destabilizing mechanism(s) resulted in changes in T_0 and sometimes T_1. Similar results for the temperature dependence of parameters were found using several cavity lengths, but only two cavity lengths are presented here for clarity. It is also noted that the room temperature device parameters calculated here are in reasonable agreement with those reported in [23], which used more cavity lengths.

B. Temperature Dependence of Threshold and Efficiency

Fig. 1 shows a linear plot of $J_{\rm th}$ and η_e with temperature, for a 20 μm $\times$ 983 μm device. The T_0 of the device was seen to be 106 K from 15 °C to 60 °C (288–333 K) and 91 K from 60 °C to 75 °C (333–348 K). The external efficiency showed a similar "kink" at 60 °C; T_1 decreased from 208 K to 104 K and was more significant for longer cavity devices. This kink in T_1 is inconsistent with conventional laser physics that requires the carrier density within the QW to pin at threshold [34], [35]. The thermal activation of an Auger process might reduce T_0, but should not affect T_1 since the carrier density above threshold should remain fixed. Activation of carrier leakage would affect both parameters since the internal efficiency is reduced both

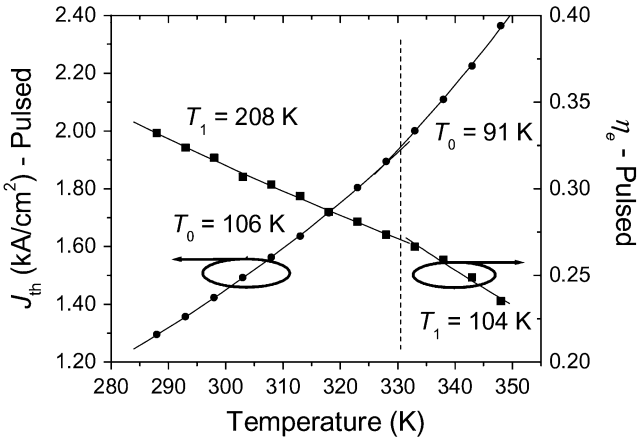

Fig. 1. Variation of $J_{\rm th}$ (circles) and η_e (squares), as a function T, for a 20 μm $\times$ 983 μm device. Exponential fits to each are also shown (lines).

above and below threshold. From (4) and (5), we see that activation of IVBA, which increases α_i, could also be responsible for these kinks. Further, IVBA would lead to more significant kinks in the longer devices, which have lower mirror loss. The sharpness of the kink and the severity of the reduction in T_1 may be overestimated due to the limited temperature measurement range in each regime. Whereas T_0 was relatively high, T_1 was significantly lower than reported for GaInNAs devices at 1.3 μm [26]. High T_0 and low T_1 values typically occur in devices with large amounts of monomolecular recombination (high T_0) and carrier leakage (low T_1).

Correlations between the temperature sensitivity (T_0 or T_1) and room temperature performance ($J_{\rm th}$ or η_e) were also investigated. For a given cavity length, T_0 was slightly positively correlated with $J_{\rm th}$, a correlation $R = 0.28$. T_0 was also slightly positively correlated with $\eta_e (R = 0.22)$. By contrast, T_1 was strongly positively correlated with both $J_{\rm th} (R = 0.97)$ and $\eta_e (R = 0.71)$. Taken together, these observations suggest a balance between the temperature stabilizing effect of monomolecular recombination and the destabilizing effects of Auger recombination and carrier leakage. Devices with higher η_e presumably have less leakage and therefore lower temperature sensitivity for the internal efficiency η_i. This produces a significantly higher T_1 but only a slightly higher T_0 since the temperature sensitivity of the gain coefficient (to be discussed in Section III-E) also influences T_0 but does not affect T_1 according to (4) and (5). This difference explains why the correlation of η_e with T_1 is stronger than that of η_e with T_0. Devices with higher room temperature $J_{\rm th}$, presumably have more monomolecular recombination and thus less temperature sensitivity. The best performing devices (lowest $J_{\rm th}$ and highest η_e) were selected for the cavity length study. These devices tended to show somewhat lower T_0 and T_1 overall.

C. Cavity Length Dependence of T_0 and T_1

The cavity length dependences of T_0 and T_1 are plotted in Figs. 2 and 3, respectively. Also shown are fits to (4) and (5) with the parameters extracted in the following sections. Fig. 2 shows

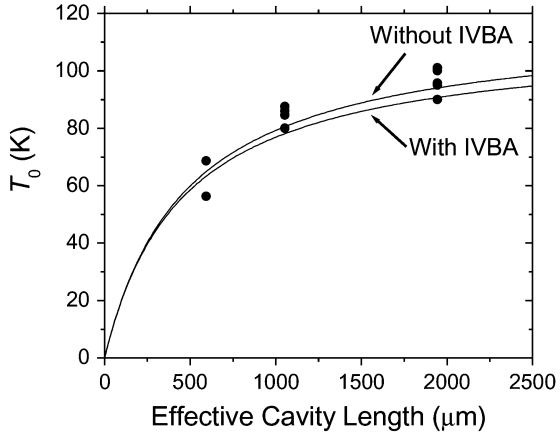

Fig. 2. Cavity length dependence of T_0 (circles). Solid lines are fits to (4) with and without IVBA.

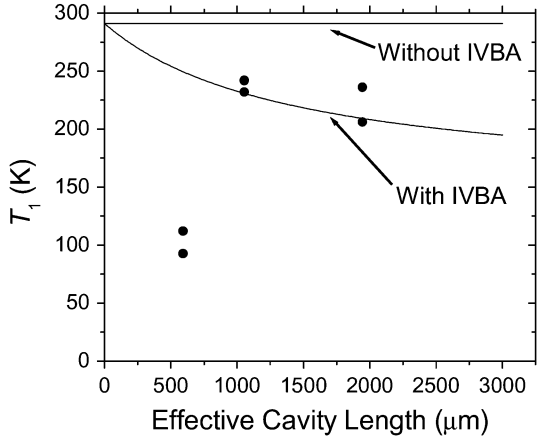

Fig. 3. Cavity length dependence of T_1 (circles). Solid lines are fits to (5) with and without IVBA.

the typical reduction in T_0 as the cavity length is decreased [17], [26]. This effect is well accounted for by the fit with (4). Mirror loss increases proportionally to $1/L$ thereby increasing the third term in (4) and reducing T_0. Also, since the threshold gain is higher for shorter devices, a larger carrier density is required to reach threshold, which increases carrier leakage and Auger recombination. The reduction in T_0 with decreased cavity length is quite similar to the cases of $In_{0.4}Ga_{0.6}As$ ($\lambda \approx 1.2$ μm) and $Ga_{0.6}In_{0.4}N_{0.005}As_{0.995}$($\lambda \approx 1.3$ μm), surrounded by GaAs–$GaAs_{0.85}P_{0.15}$ barriers [26].

The dependence of T_1 with L in Fig. 3 is not well fitted by (5) for short cavity lengths due to increased carrier leakage. Ordinarily, T_1 increases for decreasing cavity length due to the second term in (5). Here, leakage effects are dominant even at room temperature due to the greater threshold carrier density and reduced T_1 for shorter cavities. It is also clear that the reduction in T_1 is due to increased carrier leakage, as Auger recombination should not affect device efficiency above threshold. This dependence on cavity length is equivalent to regarding $T_{\eta i}$ as cavity length dependent.

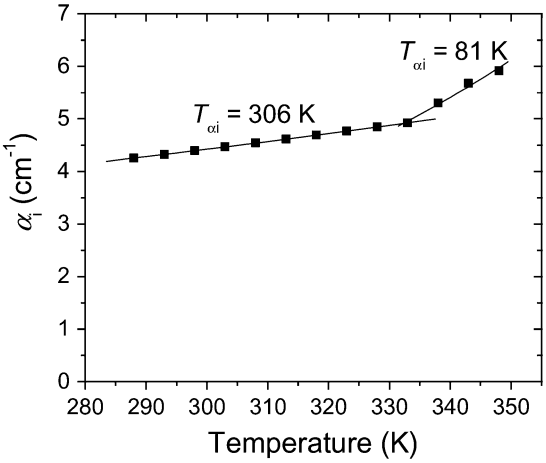

Fig. 4. Temperature dependence of α_i. (squares), with exponential fits (lines).

D. Above Threshold Parameters

Above threshold device parameters were extracted from the cavity length and temperature dependence of η_e through (2). Fig. 4 is a plot of $\alpha_i(T)$ [23]. A clear increase is observed with temperature and is consistent with the observations of IVBA in $\alpha_i(T)$ for unstrained and weakly strained InGaAs lasers on InP [7], [36]–[38]. The low temperature $T_{\alpha i}$ value of 306 K is consistent with the measurements by Henry *et al*. of IVBA with temperature in GaAs (calculated to be 307 K from their Fig. 7) [39]. Due to the minimal strain in the AlGaAs–GaAs system, it is expected that free carrier absorption processes should be approximately independent of the aluminum mole fraction [40]. The magnitude of α_i, however, was found to be three-fold higher than predicted for loss in the p-AlGaAs cladding using the data in [39]. The difference is likely due to unavoidable waveguide roughness and IVBA within the GaInNAsSb–GaNAs active region. It should be noted that Smowton and Blood predict inaccuracies in the measured value of α_i in the presence of substantial leakage [32].

The kink in $\eta_e(T)$ for the longer cavity devices caused a corresponding kink in $\alpha_i(T)$ for temperatures above 60°C, as shown in Fig. 4. It is uncertain whether the reduction in $T_{\alpha i}$ to 81 K is due to a substantial increase in IVBA or to an increase in measurement inaccuracy caused by increasing carrier leakage. Similar kinks were also observed in $g_0(T)$ and $J_{\rm tr}(T)$, as discussed in the next section, but were caused by the kinks in $J_{\rm th}(T)$ and not $\eta_e(T)$. The unexplainable decrease in $J_{\rm tr}(T)$ above the kink leads us to believe that increased measurement inaccuracy due to leakage is responsible.

IVBA does not affect $J_{\rm th}$ or T_0 appreciably, but has a significant effect on η_e and T_1. Fig. 2 shows calculations of $T_0(L)$ using (4), both with IVBA ($T_{\alpha i} = 307$ K) and without ($T_{\alpha i} = \infty$). Reduction in T_0 due to IVBA is <4 K for L up to 3000 μm. By contrast, T_1 was strongly affected by IVBA. Calculations of $T_1(L)$ with and without IVBA are plotted in Fig. 3. The effect is quite substantial for longer cavity length devices, due to reduced α_m. The IVBA term becomes more significant and T_1 is reduced by up to $\sim$30% at a cavity length of 3000 μm. In many cases, the

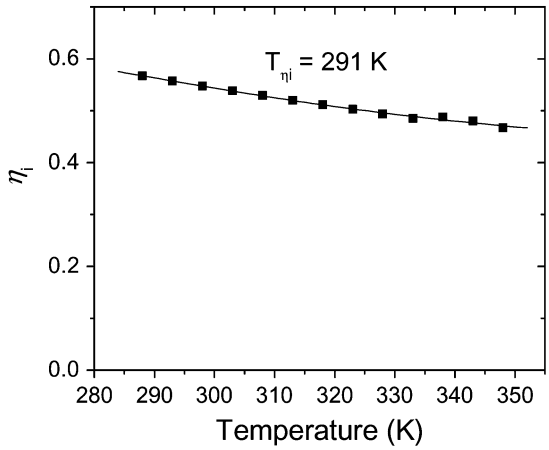

Fig. 5. Calculated η_i with temperature (squares), with exponential fit (line).

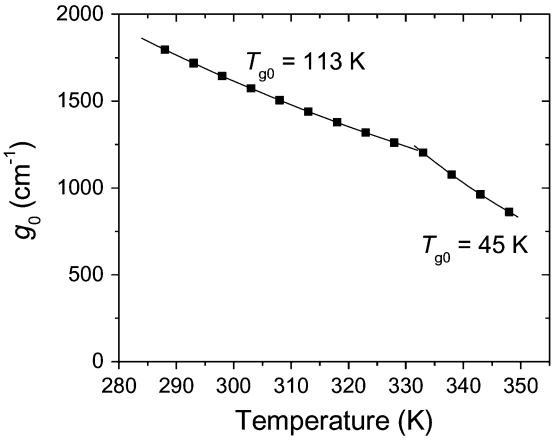

Fig. 6. Measured g_0, as a function of T (squares), with exponential fits (lines).

peak cw output power depends strongly upon T_1 [41], underscoring the importance of IVBA in long-wavelength laser design.

Fig. 5 plots η_i as a function of temperature. The value of η_i decreased from 57% to 47% over the temperature range studied, corresponding to a $T_{\eta i}$ of 291 K. This is substantially smaller than the 450 K reported for GaInNAs at 1.3-μm and 940 K for 1.2-μm InGaAs, suggesting a wavelength or nitrogen-dependent degradation [18]. The reduced temperature stability of η_i is consistent with the leakage effects observed at shorter wavelengths. No kink was present in $\eta_i(T)$. The moderately higher absolute value of η_i, as compared to those reported earlier in [23] is due to the highly reflective (HR) facet coating which effectively doubles the cavity length, but with reduced spreading resistance along the device length.

E. Below Threshold Parameters

The temperature dependence of $J_{\rm th}(L)$ was used to extract the gain parameters g_0 and $J_{\rm tr}$. The values of $\eta_i(T)$ and $\alpha_i(T)$ found in the previous section were used in the calculations of $J_{\rm tr}$. Fig. 6 is a plot of $g_0(T)$. The peak gain coefficient is an extremely insightful parameter as it is seen to degrade rapidly with temperature. Between 15 °C and 60 °C, g_0 decreased from 1500 to 1250 cm^{-1}. The low characteristic temperature $T_{g0} = 113$ K (15 °C–60 °C) is indicative of thermal broadening of the gain spectrum and/or carrier leakage. A dramatic reduction in T_{g0} to 45 K was observed at higher temperatures. Tansu and Mawst have shown strong evidence of hole leakage in 1.3-μm GaInNAs lasers [19]. Through the use of GaAsP barriers surrounding the QW to suppress hole leakage, they have shown a simultaneous reduction in $J_{\rm th}$ and improvement in T_0. Moreover, they found a further reduction of $J_{\rm th}$ and improvement in T_0 with increased phosphorous mole fraction in the barriers surrounding the QW, demonstrating the presence of hole leakage [42]. The dramatically reduced T_{g0}, as compared to 350 K for GaInNAs at 1.3-μm and 2000 K for 1.2-μm InGaAs, is strong evidence of increased carrier leakage at 1.5 μm. The simultaneous observations of a relatively high T_0 and carrier leakage effects also implies a substantial amount of monomolecular recombination current in the lasers. This is in agreement with the Z-parameter measurements in Section IV. The enhanced temperature sensitivity of the threshold current is a rather unexpected result at longer wavelengths as the valence band offset is expected to be larger due to the presence of antimony into the QW. However, the QW is surrounded by strain compensating GaNAs barriers, which reduce both the effective valence and conduction band offsets. As will be discussed in Section IV, the thermionic escape times of electrons and holes into the GaNAs barriers are quite short for the compositions studied here.

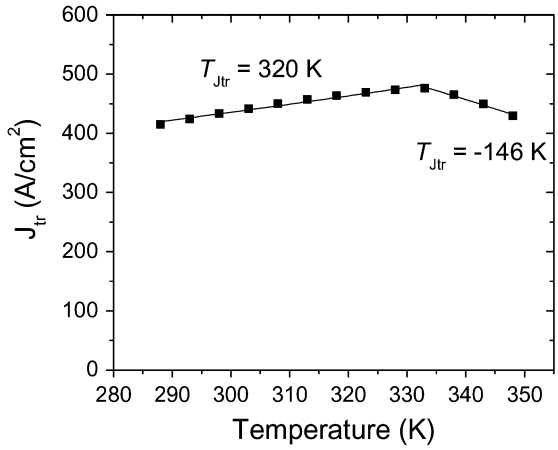

Fig. 7. Dependence of $J_{\rm tr}$ upon temperature (squares), with exponential fits (lines).

The temperature dependence of $J_{\rm tr}$ is plotted in Fig. 7. The value of $T_{\rm tr}$ was determined to be 320 K at low temperatures and -146 K, at high temperatures. This anomalous temperature behavior arises from the ratio $\alpha_i(T)/\Gamma \cdot g_0(T)$ and may be due to increased measurement inaccuracy. Tansu and coworkers have found [17], through a variation in the O'Reilly and Silver analysis [9], that a device dominated by radiative recombination has $T_{\rm tr}$ in the range 150–350 K. The relatively high value reported here, 320 K, however, is more consistent with a large monomolecular component to the transparency current ($T_{\rm tr} \approx$ 300–400 K), rather than the radiative case ($T_{\rm tr} \approx$ 150–300 K) or the more temperature dependent Auger recombination ($T_{\rm tr} \approx$ 75–100 K).

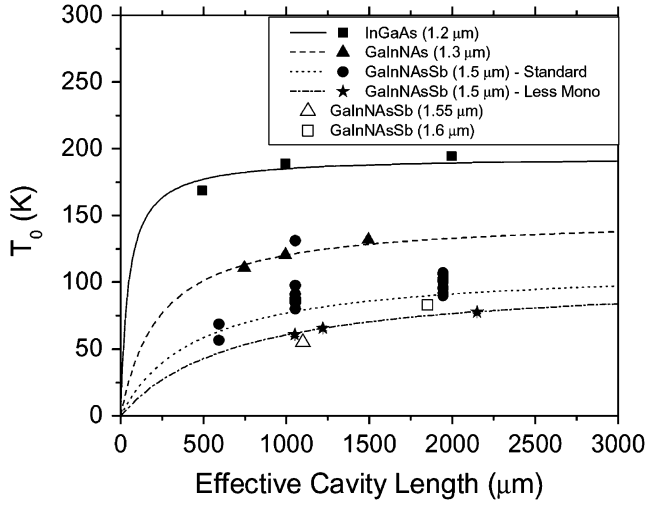

Fig. 8. Cavity length dependence of T_0 for GaIn(N)As(Sb) lasers emitting at different wavelengths [17], [18].

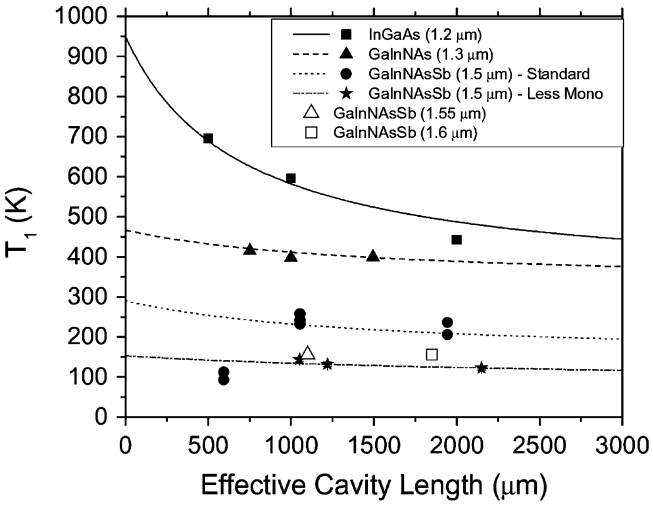

Fig. 9. Cavity length dependence of T_1 for GaIn(N)As(Sb) lasers emitting at different wavelengths [17], [18].

F. Wavelength Dependence of T_0 and T_1

The cavity length dependences of T_0 and T_1 for various GaIn–NAsSb compositions (lasing wavelengths) are plotted in Figs. 8 and 9, respectively. The 1.2-μm InGaAs and 1.3-μm GaInNAs lasers were grown by Tansu and coworkers and reported in [17] and [18], while the remaining data comes from our wafers. The 1.5-μm GaInNAsSb lasers consist of the devices discussed in Section III-C, labeled "Standard" and our newer generation of 1.5-μm devices, labeled "Less Mono," which have 2x lower thresholds as discussed in [43]. Reduced monomolecular recombination was identified as the source of lower thresholds through Z-parameter measurements. It also naturally explains the increased temperature sensitivity, i.e., lower T_0 and T_1.

The typical values for T_0 and T_1 are significantly worse at 1.5 μm compared to the values at 1.2 and 1.3 μm for two reasons. First, Auger recombination is drastically enhanced in long wavelength operation. Second, the large GaAsP barriers used in the 1.2- and 1.3-μm lasers significantly reduce carrier leakage whereas the much smaller GaNAs barriers provide less carrier confinement and also have more defects—both of which enhance recombination outside of the quantum well.

The preliminary 1.55-μm and 1.6-μm GaInNAsSb lasers have $2\times$ and $3\times$ higher thresholds, respectively, than the 1.5-μm "Standard," in addition to having greater temperature sensitivity. The growth conditions of these very long wavelength lasers still require much optimization. The cause of the degradation in performance is currently under investigation, but it is believed to be an increase in monomolecular, Auger recombination, and carrier leakage compared to the "Standard" sample.

IV. Supporting Measurement Techniques

Three measurement techniques are briefly reviewed in this section to confirm the findings of the cavity length study. First, Z-parameter measurements were performed and show that the "kinks" in $J_{\rm th}(T)$ and $\eta_e(T)$ are likely caused by the turn-on of a process that depends strongly on the carrier density such as Auger recombination or carrier leakage. Second, Fermi level pinning in the active region was investigated through spontaneous emission measurements. Very weak pinning of nonlasing transitions was observed above threshold. This supports the conclusion that carrier leakage is significant and the carrier density continues to increase substantially above threshold. These techniques are discussed in detail elsewhere [31] and are presented here as supporting evidence. Third, the band offsets between the GaInNAsSb QW and GaNAs barriers have been measured with X-ray photoemission spectroscopy (XPS) [44], photoreflectance (PR) [45], and absorption [31]. The techniques all indicate the band offsets are approximately equal for electrons and holes. For the given offsets, thermionic escape times were found to be much less than the radiative lifetime. The combination of all of the measurement techniques allows for a more complete understanding of the temperature sensitivity of 1.5-μm GaInNAsSb–GaNAs lasers.

A. Z-Parameter

To investigate the kink in T_0 at elevated temperatures and the role of monomolecular recombination, a focused ion beam was used to mill a 5 μm $\times$ 10 μm window in the top metal of a 10 μm $\times$ 750 μm device in a geometry similar to those reported in [7] and [27]. The spontaneous emission was collected onto a fiber and the integrated emission rate (SPE) was measured with a lightwave multimeter. In this vertical configuration, only TE polarized spontaneous emission was collected, but due to the large heavy hole to light hole splitting due to strain and effective mass, the heavy hole transitions dominate and the collected SPE well represents the total spontaneous emission. The local Z-parameter, described in [7] and [31], is the gradient of the $\ln(J)$ versus $\ln(\mathrm{SPE}^{1/2})$ and is typically assumed to range from $Z = 1$ where monomolecular recombination dominates to $Z = 3$ where Auger recombination dominates. Departure from $Z = 2$ indicates non-radiative recombination. Below threshold, where stimulated emission is weak, $Z \approx 1J_{\rm Mono}/J_{\rm Tot} + 2J_{\rm Rad}/J_{\rm Tot} + 3J_{\rm Aug}/J_{\rm Tot}$, where $J_{\rm Mono}$,

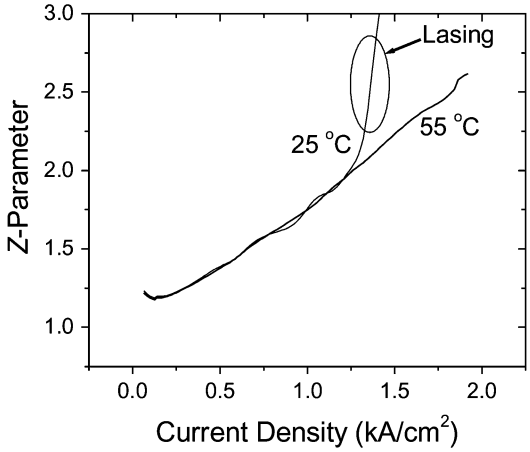

Fig. 10. Measurement of the local Z-parameter with bias current density at 20 °C and 55 °C verifying the presence of monomolecular recombination, as well as another process that depends strongly upon the carrier density.

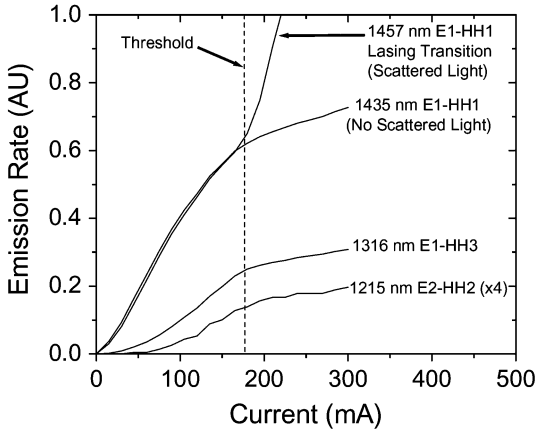

Fig. 11. Room temperature spontaneous emission rates, as a function of pulsed drive current, for several important transitions. Transitions shown are E1-HH1 (with and without scattered laser light), E1-HH3, and E2-HH2. Note that the emission continues to increase rapidly even above threshold (denoted with dotted line).

J_{Rad}, J_{Aug}, and J_{Tot} are the monomolecular, radiative, Auger, and total currents, respectively. The instantaneous Z-parameter is plotted in Fig. 10 at 25 °C and 55 °C. The Z–J curves are quite similar at both temperatures and indicate significant monomolecular recombination. This is further evidenced by the wide range of bias currents where $Z < 2$, indicating large portions of the current are lost through monomolecular recombination. It is safely concluded that monomolecular recombination dominates the threshold current near room temperature (i.e., low J_{th}). At elevated biases $\sim$1.5–2 kA/cm^2, consistent with J_{th} at elevated temperatures, the Z-parameter rose well above 2.0, indicating the turn-on of another non-radiative loss mechanism. This is consistent with the kink in T_0, which is, therefore, attributed to the rise in Auger recombination and/or carrier leakage.

It should be noted that this technique cannot distinguish between leakage current and Auger recombination. The Z-parameter for pure Auger recombination depends upon the carrier densities (degenerate or nondegenerate) and the type of Auger transition involved, but generally should cause $Z \approx 3$–4 [31]. Carrier leakage into the barriers and waveguiding regions could show Z ranging widely from 1 to 4 due to the carrier density dependence [46], [31]. Even in the presence of large monomolecular or radiative recombination, the Z-parameter may show $Z > 2$ in lasers with minimal Auger recombination, if leakage is significant.

B. Spontaneous Emission

Spontaneous emission spectra were also collected at normal incidence to the QW through the milled window. The spontaneous emission spectrum escaping from the ridge waveguide was collected onto a fiber and spectrally resolved in an optical spectrum analyzer. Measurements were performed under low duty cycle operation to eliminate heating effects. As shown in Fig. 11, the emission efficiency above threshold ($\sim$175 mA) from nonlasing transitions was weakly pinned $\sim$40% of the below threshold efficiency. Only a few main transitions are reproduced here, but the behavior of other transitions was similar. Higher level transitions also pinned more weakly and virtually no pinning was observed in the GaNAs barrier signal (not shown). The continual increase in spontaneous emission above threshold is an independent verification of carrier leakage in these devices. Visible InGaP lasers, which also suffer from electron leakage into the p-type waveguiding regions, show similarly weak pinning above threshold [27]. Much stronger pinning, $\sim$10% emission ratio, is typical in AlGaAs–GaAs semiconductor lasers where carrier leakage is not a significant issue [47].

C. Band Offsets

Band offset measurements of GaInNAsSb–GaNAs were performed using several techniques: XPS, PR, and absorption. For the devices studied here, the effective band offset ratio was found to be $\Delta E_c : /\Delta E_v \approx 56 : 44$ using absorption and is consistent with the other techniques. Between the QW and barriers, $\Delta E_c = 164$ meV and $\Delta E_v = 115$ meV (between the QW heavy hole and barrier light hole levels) were found. The calculated thermionic emission times out of the QW, for both electrons and holes, were found to be quite small, an order of magnitude less than the total recombination lifetime $\sim$0.8 ns measured by relative intensity noise techniques [48]. Moreover, the electron and hole escape times are heavily temperature dependent [49] and degrade from 42 to 8 ps and 60 to 13 ps, respectively, from 10 °C to 90 °C. The hole escape time may even be 3–5$\times$ shorter if there is efficient heavy hole to light hole scattering. Therefore, carriers are able to easily escape from the QW structure into the GaNAs barriers and recombine radiatively and nonradiatively, thus reducing η_i.

V. Conclusion

Through the characterization techniques presented here, evidence of monomolecular recombination, IVBA, and carrier leakage has been found. Auger recombination likely also plays a role, but it is not possible to answer definitively at present. Auger recombination and carrier leakage are not mutually exclusive

effects, however, and can even enhance one another [50], [51]. Monomolecular recombination provides an artificial stabilization of T_0 as evidenced by the significant temperature sensitivity of η_i, above threshold. Reduction of monomolecular recombination is relatively straightforward and likely involves further reduction in plasma-related damage and other optimization of the growth technique [52]. IVBA does not significantly degrade $J_{\rm th}$ or T_0, but strongly reduces T_1. This effect may be suppressed by reducing the threshold carrier density, the doping of the cladding layer, and the scattering loss component of α_i through improved lithography and etching. Auger effects could be reduced by optimizing the band structure, similar to the incorporation of strain in InGaAsP–InP devices. This would most likely involve changing the relative indium, nitrogen, and antimony mole fractions to suppress the dominant Auger process(es). Such an approach is promising due to the unparalleled degrees of freedom afforded with a quinary active layer.

Several traits in the temperature behavior of these devices have indicated carrier leakage: 1) the reduced T_1 at short cavity lengths that can only be explained by assuming a cavity length dependent $T_{\eta i}$; 2) the low T_{g0} and $T_{\eta i}$; 3) the poor η_i and $\eta_{\rm e}$; 4) the reduction in T_0 at short cavity lengths; 5) the weak pinning of higher level transitions at threshold; and 6) the short thermionic escape times from the QW. While the absolute magnitudes of T_{g0} (100–200 K) and $T_{\eta{\rm inj}}$ (200–300 K) vary somewhat depending upon the devices chosen, these values are much lower than those reported for InGaAs lasing at $\sim$1.2 μm and GaInNAs at 1.3 μm [26].

The carrier leakage mechanism remains an open question, however. Due to the high energy barriers between the confined QW levels and the AlGaAs cladding, diffusive leakage into the AlGaAs waveguiding layers is quite low. Moreover, the high electrical conductivity of even moderately doped AlGaAs makes drift leakage into the AlGaAs an unlikely mechanism as well. Applying the analysis of Bour and coworkers [14], the overall contribution of drift and diffusive leakage for both electrons and holes into the AlGaAs waveguiding regions are $<$1 A/cm^2. Another potential mechanism is non-radiative recombination in the GaNAs barriers. As reported in [53] and [54], GaNAs material quality is quite poor in the regime dictated by the QW growth conditions ($\sim$440 °C at a growth rate of 0.3 μm/h) and contains many traps [12], [55], [56]. The typical peak photoluminescence efficiency is $\sim$25$\times$ weaker from a GaNAs QW compared to a GaInNAsSb QW [54]. These barriers may serve as sinks of carriers though thermionic emission or tunneling. The short thermionic escape times of carriers into the barriers, in concert with Shockley–Read–Hall (SRH) recombination, creates a complex loss mechanism that would degrade the temperature stability of the lasers and explain the weak pinning observed in spontaneous emission spectra above threshold. The SRH recombination rate was estimated using electron trap densities from deep level transient spectroscopy ($\sim 10^{17}$ cm^{-3}), capture cross-sections (10^{-15}–10^{-14} cm^{-2}), and the threshold carrier densities in the barriers (1.5×10^{16} cm^{-3} for electrons and 3.0×10^{16} cm^{-3} for holes). This mechanism contributes $\sim$10–100 A/cm^2 at threshold, depending on the exact value of the capture cross-section, and may explain the weak pinning observed in the spontaneous emission. The trap density is much larger than the barrier electron concentration and the traps may not all be filled at threshold, leading to a recombination path that can increase above threshold. However, this effect alone cannot explain the magnitude of $J_{\rm th}$, consistent with the $T_{\rm tr}$ and Z-parameter data that show significant monomolecular recombination within the QW. Near room temperature, this is the dominant carrier loss mechanism at threshold ($\sim$60%).

There are several techniques that mitigate this effect by reducing the defects surrounding the QW. One solution is GaAs barriers, but this is generally less desirable as the barriers do not provide any strain compensation. Asymmetric barriers, one GaNAs barrier and one GaAs barrier, could be a compromise to reduce the effect by approximately half while retaining much of the strain compensation. More promising approaches are antimony co-doping [57] to improve the GaNAs quality or employing GaAsP barriers [58], [17]. GaAsP barriers are the most advantageous in terms of material quality, strain compensation, and increased band offsets.

By examining the temperature and cavity length behavior of 1.5-μm GaInNAsSb lasers, in conjunction with supporting techniques, we have identified the effects of carrier leakage, monomolecular recombination, IVBA, and possibly Auger recombination. It is believed that with further growth improvements, GaInNAsSb active layers will find future application in GaAs-based VCSEL sources and high-power edge-emitting lasers to pump Raman amplifiers and high-energy solid-state lasers.

ACKNOWLEDGMENT

The authors would like to thank Prof. A. R. Adams, University of Surrey, Prof. N. Tansu, Lehigh University, Philadelphia, PA, and Dr. D. P. Bour, Agilent Technologies, Palo Alto, CA, for many useful discussions regarding Auger recombination, carrier leakage, IVBA, and the Z-parameter. R. Kudrawiec is acknowledged for graciously providing PR and band-offset data prior to publication. The authors also wish to thank S. Zou of Santur Corporation, for assistance in wafer thinning and facet coatings. The authors also thank Dr. A. Moto of Sumitomo Electric Industries for helpful discussions and donation of substrates.

REFERENCES

[1] M. Kondow, T. Kitatani, S. Nakatsuka, M. C. Larson, K. Nakahara, Y. Yazawa, M. Okai, and K. Uomi, "GaInNAs: A novel material for long-wavelength semiconductor lasers," *IEEE J. Sel. Topics Quantum Electron.*, vol. 3, no. 6, pp. 719–730, Jun. 1997.

[2] C. W. Coldren, M. C. Larson, S. G. Spruytte, and J. S. Harris, "1200 nm GaAs-based vertical cavity lasers employing GaInNAs multiquantum well active regions," *Electron. Lett.*, vol. 36, pp. 951–952, May 2000.

[3] W. Ha, V. Gambin, S. Bank, M. Wistey, H. Yuen, S. Kim, and J. S. Harris Jr., "Long-wavelength GaInNAs(Sb) lasers on GaAs," *IEEE J. Quantum Electron.*, vol. 38, no. 9, pp. 1260–1267, Sep. 2002.

[4] L. H. Li, V. Sallet, G. Patriarche, L. Largeau, S. Bouchoule, K. Merghem, L. Travers, and J. C. Harmand, "1.5 μm laser on GaAs with GaInNAsSb quinary quantum well," *Electron. Lett.*, vol. 39, pp. 519–520, Mar. 2003.

[5] D. Gollub, S. Moses, M. Fischer, and A. Forchel, "1.42 μm continuous-wave operation of GaInNAs laser diodes," *Electron. Lett.*, vol. 39, pp. 777–778, May 2003.

[6] S. R. Bank, M. A. Wistey, H. B. Yuen, L. L. Goddard, W. Ha, and J. S. Harris Jr., "Low-threshold CW GaInNAsSb/GaAs laser at 1.49 μm," *Electron. Lett.*, vol. 39, pp. 1445–1446, Oct. 2003.

[7] A. F. Phillips, S. J. Sweeney, A. R. Adams, and P. J. A. Thijs, "The temperature dependence of 1.3- and 1.5-μm compressively strained InGaAs(P) MQW semiconductor lasers," *IEEE J. Sel. Topics Quantum Electron.*, vol. 5, no. 3, pp. 401–412, May/Jun. 2002.

[8] P. J. A. Thijs, L. F. Tiemeijer, P. I. Kuindersma, J. J. M. Binsma, and T. Van Dongen, "High-performance 1.5 μm wavelength InGaAs–InGaAsP strained quantum well lasers and amplifiers," *IEEE J. Quantum Electron.*, vol. 27, no. 6, pp. 1426–1439, Jun. 1991.

[9] E. P. O'Reilly and M. Silver, "Temperature sensitivity and high temperature operation of long wavelength semiconductor lasers," *Appl. Phys. Lett.*, vol. 63, no. 6, pp. 3318–3320, Dec. 1993.

[10] W. Shan, W. Walukiewicz, J. W. Ager III, E. E. Haller, J. F. Geisz, D. J. Friedman, J. M. Olson, and S. R. Kurtz, "Band anticrossing in GaInNAs alloys," *Phys. Rev. Lett.*, vol. 82, pp. 1221–1224, Feb. 1999.

[11] M. Hetterich, M. D. Dawson, A. Y. Egorov, D. Bernklau, and H. Riechert, "Electronic states and band alignment in GaInNAs/GaAs quantum-well structures with low nitrogen content," *Appl. Phys. Lett.*, vol. 76, pp. 1030–1032, Feb. 2000.

[12] P. Krispin, S. G. Spruytte, J. S. Harris, and K. H. Ploog, "Electrical depth profile of p-type GaAs/Ga(As, N)/GaAs heterostructures determined by capacitance-voltage measurements," *J. Appl. Phys.*, vol. 88, pp. 4153–4158, Oct. 2000.

[13] M. Kondow, K. Uomi, A. Niwa, T. Kitatani, S. Watahiki, and Y. Yazawa, "GaInNAs: A novel material for long-wavelength-range laser diodes with excellent high-temperature performance," *Jpn. J. Appl. Phys. Suppl.*, vol. 35, pp. 1273–1275, Feb. 1996.

[14] D. P. Bour, D. W. Treat, R. L. Thornton, R. S. Geels, and D. F. Welch, "Drift leakage current in AlGaInP quantum-well lasers," *IEEE J. Quantum Electron.*, vol. 29, no. 5, pp. 1337–1343, May 1993.

[15] M. Kondow, S. Natatsuka, T. Kitatani, Y. Yazawa, and M. Okai, "Room-temperature continuous-wave operation of GaInNAs/GaAs laser diode," *Electron. Lett.*, vol. 32, pp. 2244–2245, Nov. 1996.

[16] R. S. Muller and T. I. Kamins, *Device Electronics for Integrated Circuits*, 2nd ed., New York: Wiley, 1986, pp. 222–226.

[17] N. Tansu, Y. L. Chang, T. Takeuchi, D. P. Bour, S. W. Corzine, M. R. T. Tan, and L. J. Mawst, "Temperature analysis and characteristics of highly strained InGaAs–GaAsP-GaAs ($\lambda > 1.17$ μm) quantum-well lasers," *IEEE J. Quantum Electron.*, vol. 38, pp. 640–651, Jun. 2002.

[18] N. Tansu and L. J. Mawst, "Temperature sensitivity of 1300-nm InGaAsN quantum-well lasers," *IEEE Photon. Technol. Lett.*, vol. 14, no. 8, pp. 1052–1054, Aug. 2002.

[19] N. Tansu, J. Y. Yeh, and L. J. Mawst, "Experimental evidence of carrier leakage in InGaAsN quantum-well lasers," *Appl. Phys. Lett.*, vol. 83, pp. 2112–2114, Sep. 2003.

[20] R. Fehse, S. Tomic, A. R. Adams, S. J. Sweeney, E. P. O'Reilly, A. Andreev, and H. Riechert, "A quantitative study of radiative, Auger, and defect related recombination processes in 1.3-μm GaInNAs-based quantum-well lasers," *IEEE J. Sel. Topics Quantum Electron.*, vol. 8, no. 4, pp. 801–810, Jul./Aug. 2002.

[21] M. C. Wang, K. Kash, C. E. Zah, R. Bhat, and S. L. Chuang, "Measurement of non-radiative Auger and radiative recombination rates in strained-layer quantum-well systems," *Appl. Phys. Lett.*, vol. 62, pp. 166–168, Jan. 1993.

[22] R. Fehse, S. J. Sweeney, A. R. Adams, E. P. O'Reilly, A. Y. Egorov, H. Riechert, and S. Illek, "Insights into carrier recombination processes in 1.3 μm GaInNAs-based semiconductor lasers attained using high pressure," *Electron. Lett.*, vol. 37, pp. 92–93, Jan. 2001.

[23] S. R. Bank, M. A. Wistey, L. L. Goddard, H. B. Yuen, and J. S. Harris Jr., "Low-threshold, continuous-wave, 1.5 μm GaInNAsSb lasers grown on GaAs," *IEEE J. Quantum Electron.*, vol. 40, no. 6, pp. 656–664, Jun. 2004.

[24] J. Y. Yeh, N. Tansu, and L. J. Mawst, "Temperature-sensitivity analysis of 1360-nm dilute-nitride quantum-well lasers," *IEEE Photon. Technol. Lett.*, vol. 16, no. 3, pp. 741–743, Mar. 2004.

[25] J. S. Harris Jr., "GaInNAs long-wavelength lasers: Progress and challenges," *Semicond. Sci. Technol.*, vol. 17, pp. 880–891, Jul. 2002.

[26] N. Tansu and L. J. Mawst, "Low-threshold strain-compensated InGaAs(N) ($\lambda = 1.19$–1.31 μm) quantum-well lasers," *IEEE Photon. Techol. Lett.*, vol. 14, no. 4, pp. 444–446, Apr. 2002.

[27] P. M. Smowton and P. Blood, "The differential efficiency of quantum-well lasers," *IEEE J. Sel. Topics Quantum Electron.*, vol. 3, no. 2, pp. 491–498, Mar./Apr. 1997.

[28] S. L. Chuang, *Physics of Optoelectronic Devices*. New York: Wiley, 1995, pp. 432–435.

[29] ——, *Physics of Optoelectronic Devices*. New York: Wiley, 1995, p. 401.

[30] L. A. Coldren and S. W. Corzine, *Diode Lasers and Photonic Integrated Circuits*. New York: Wiley, 1995, pp. 29–30.

[31] L. L. Goddard, S. R. Bank, M. A. Wistey, H. B. Yuen, Z. Rao, and J. S. Harris Jr., "Recombination, gain, band structure, efficiency, and reliability of 1.5-μm GaInNAsSb/GaAs lasers," *J. Appl. Phys.*, vol. 97, p. 083101-1-15, Apr. 2005.

[32] P. M. Smowton and P. Blood, "On the determination of internal optical mode loss of semiconductor lasers," *Appl. Phys. Lett.*, vol. 70, pp. 2365–2367, May 1997.

[33] ——, "Fermi level pinning and differential efficiency in GaInP quantum well lasers," *Appl. Phys. Lett.*, vol. 70, pp. 1073–1075, Mar. 1997.

[34] S. L. Chuang, *Physics of Optoelectronic Devices*. New York: Wiley, 1995, p. 399.

[35] L. A. Coldren and S. W. Corzine, *Diode Lasers and Photonic Integrated Circuits*. New York: Wiley, 1995, pp. 40–41.

[36] M. Asada, A. R. Adams, K. E. Stubkjaer, Y. Suematsu, Y. Itaya, and S. Arai, "The temperature dependence of the threshold current of GaInAsP/InP DH lasers," *IEEE J. Quantum Electron.*, vol. QE-17, no. 5, pp. 611–619, May 1981.

[37] G. Fuchs, J. Horer, A. Hangleiter, V. Harle, F. Scholz, R. W. Glew, and L. Goldstein, "Intervalence band absorption in strained and unstrained InGaAs multiple quantum well structures," *Appl. Phys. Lett.*, vol. 60, pp. 231–233, Jan. 1992.

[38] Y. Zao, J. S. Osinski, P. Grodzinski, P. D. Dapkus, W. C. Rideout, W. F. Sharfin, J. Schlafer, and F. D. Crawford, "Experimental study of Auger recombination, gain, and temperature sensitivity of 1.5 μm compressively strained semiconductor lasers," *IEEE J. Quantum Electron.*, vol. 29, pp. 1565–1575, Jun. 1993.

[39] C. H. Henry, R. A. Logan, F. R. Merritt, and J. P. Luongo, "The effect of intervalence band absorption on the thermal behavior of InGaAsP lasers," *IEEE J. Quantum Electron.*, vol. QE-19, no. 6, pp. 947–952, Jun. 1983.

[40] W. Szuszkiewicz, "Free carrier effects and intervalence-band absorption in AlGaAs," in *Properties of Aluminum Gallium Arsenide*, S. Adachi, Ed. London, U.K.: INSPEC, 1993, p. 145.

[41] D. Botez, "Design considerations and analytical approximations for high continuous-wave power, broad-waveguide diode lasers," *Appl. Phys. Lett.*, vol. 74, pp. 3102–3104, May 1999.

[42] N. Tansu and L. J. Mawst, "Current injection efficiency of InGaAsN quantum-well lasers," *J. Appl. Phys.*, vol. 97, pp. 054502-1–18, Mar. 2005.

[43] L. Goddard, S. Bank, M. Wistey, H. Yuen, and J. S. Harris Jr., "High performance GaInNAsSb/GaAs lasers at 1.5 μm," *Proc. SPIE*, vol. 5738, pp. 180–191, Apr. 2005.

[44] H. B. Yuen "GaInNAsSb-GaAs Band Offsets From XPS," unpublished.

[45] R. Kudrawiec, H. B. Yuen, K. Ryczko, J. Misciewicz, S. R. Bank, M. A. Wistey, H. P. Bae, and J. S. Harris Jr., "Photoreflectance and photoluminescence investigations of a step-like GaInNAsSb/GaAsN/GaAs quantum well tailored at 1.5 μm: The energy level structure and the Stokes shift," *J. Appl. Phys.*, vol. 97, p. 053515-1-7, Mar. 2005.

[46] R. Olshansky, C. B. Su, J. Manning, and W. Powazinik, "Measurement of radiative and nonradiative recombination rates in InGaAsP and AlGaAs light sources," *IEEE J. Quantum Electron.*, vol. QE-20, no. 8, pp. 838–854, Aug. 1984.

[47] R. Nagarajan and J. E. Bowers, "Effects of carrier transport on injection efficiency and wavelength chirping in quantum-well lasers," *IEEE J. Quantum Electron.*, vol. 29, no. 6, pp. 1601–1608, Jun. 1993.

[48] J. S. Harris Jr., M. A. Wistey, S. R. Bank, V. Lordi, L. L. Goddard, H. Bae, and H. B. Yuen, "Long-wavelength dilute nitride-antimonide lasers," in *Dilute Nitride Semiconductors*, M. Henini, Ed. Amsterdam, The Netherlands: Elsevier, Jan. 2005, pp. 507–578.

[49] H. Schneider and K. V. Klitzing, "Thermionic emission and Gaussian transport of holes in GaAs/Al_xGa_{1-x} As multiple-quantum-well structure," *Phys. Rev. B*, vol. 38, pp. 6160–6165, Sep. 1988.

[50] H. C. Casey Jr., "Temperature dependence of the threshold current density in InP-$Ga_{0.28}In_{0.72}As_{0.6}P_{0.4}$ ($\lambda = 1.3$ μm) double heterostructure lasers," *Appl. Phys. Lett.*, vol. 56, pp. 1959–1964, Oct. 1984.

[51] A. R. Adams, private communication, Aug. 2003.

[52] J. S. Harris, S. R. Bank, M. A. Wistey, and H. B. Yuen, "GaInNAs(Sb) long wavelength communications lasers," *Proc. Inst. Elect. Eng.*, vol. 151, pp. 407–416, Oct. 2004.

[53] J. S. Wang, A. R. Kovsh, L. Wei, J. Y. Chi, Y. T. Wu, P. Y. Wang, and V. M. Ustinov, "MBE growth of high-quality GaAsN bulk layers," *Nanotechnol.*, vol. 12, pp. 430–433, Nov. 2001.
[54] H. B. Yuen, S. R. Bank, M. A. Wistey, J. S. Harris Jr., and A. Moto, "Comparison of GaNAsSb and GaNAs as quantum well barriers for GaInNAsSb optoelectronic devices operating at 1.3–1.55 μm," *J. Appl. Phys.*, vol. 96, pp. 6375–6381, Dec. 2004.
[55] P. Krispin, S. G. Spruytte, J. S. Harris, and K. H. Ploog, "Electron traps in Ga(As,N) layers grown by molecular-beam epitaxy," *Appl. Phys. Lett.*, vol. 80, pp. 2120–2122, Mar. 2002.
[56] P. Krispin, V. Gambin, J. S. Harris, and K. H. Ploog, "Nitrogen-related electron traps in Ga(As,N) layers ($\leq 3\%$ N)," *J. Appl. Phys.*, vol. 93, pp. 6095–6099, May 2003.
[57] H. B. Yuen, M. J. Seong, R. Kudrawiec, S. Yoon, S. R. Bank, M. A. Wistey, J. Misciewicz, and J. S. Harris Jr., "Improved optical quality from indium-free GaNAsSb in the dilute Sb limit," *J. Appl. Phys.*, vol. 97, p. 113510-1-5, May 2005.
[58] M. Hetterich, M. D. Dawson, A. Yu. Egorov, D. Bernklau, H. Riechert, S. W. Bland, J. I. Davies, and M. D. Geen, "Comparison of GaInNAs/GaAs and strain-compansated InGaAs/GaAsP quantum wells for 1200–1300nm diode lasers," in *Proc. 12th Annu. Meeting IEEE Lasers and Electro-Optics Society (LEOS)*, vol. 1, 1999, p. 368.

Seth R. Bank (S'95) received the B.S. degree from the University of Illinois at Urbana-Champaign (UIUC) and the M.S. degree from Stanford University, Stanford, CA, both in electrical engineering. He is currently working toward the Ph.D. degree at Stanford University. While at UIUC, he studied the fabrication of InGaP–GaAs and InGaAs–InP HBTs.

His research currently focuses on the MBE growth, fabrication, and device physics of long-wavelength VCSELs and high-power edge-emitting lasers in the GaInNAsSb-GaAs material system. He has coauthored over 50 papers and presentations.

Mr. Bank has received the 2004 Electronic Materials Conference Student Award, the 2005 Ross N. Tucker Award from the Electronics Materials Symposium, the Gerald L. Pearson Memorial Fellowship (Stanford), and the John Bardeen Scholarship (UIUC).

Lynford L. Goddard (S'04) was born in Redwood City, CA, on June 10, 1975. He received the B.S. degree in mathematics and physics and the M.S. degree in electrical engineering from Stanford University, Stanford, CA, in 1998 and 2003, respectively. His undergraduate honors thesis covered linear differential operators. He is currently working toward the Ph.D. degree in physics at Stanford University, where his research areas are GaInNAsSb–GaAs laser characterization and modeling.

At Xerox Palo Alto Research Center, he characterized the gain of 400-nm InGaN lasers during life testing.

Mark A. Wistey (S'93) received the B.S. degree in electrical engineering from Montana State University, Bozeman, and the M.S. degree from Stanford University, Stanford, CA, where he is currently working toward the Ph.D. degree.

His current research is on long-wavelength optoelectronics and VCSELs on GaAs, using dilute nitrides such as GaInNAs, grown by MBE. He is the coauthor of over 70 papers and presentations related to dilute nitrides.

Mr. Wistey is a recipient of a 2003 Student Award from the North American Conference on Molecular Beam Epitaxy and a 2004 Ross Tucker Award.

Homan B. Yuen (S'04) received the B.A. degree in physics from the University of California at Berkeley in 2000, and the M.S. degree in electrical engineering from Stanford University, Stanford, CA, in 2003. He is currently working toward the Ph.D. degree in materials science and engineering at Stanford University, studying the GaInNAsSb–GaAs material system for applications in long-wavelength optoelectronic devices.

Mr. Yuen received a 2004 Graduate Student Award from the Materials Research Society.

James S. Harris, Jr. (S'66–M'68–SM'77–F'88) received the B.S., M.S., and Ph.D. degrees in electrical engineering from Stanford University, Stanford, CA, in 1964, 1965, and 1969, respectively.

He is currently the James and Ellenor Chesebrough Professor of Electrical Engineering, Applied Physics and Materials Science at Stanford University. In 1969, he joined the Rockwell International Science Center, Thousand Oaks, CA, where he was one of the key contributors to ion implantation, MBE, and heterojunction devices, leading to their preeminent position in GaAs technology. In 1980, he became Director of the Optoelectronics Research Department and in 1982, he joined the Solid State Electronics Laboratory, Stanford University, as a Professor of electrical engineering. He served as Director of the Solid State Electronics Laboratory (1984–1998) and Director of the Joint Services Electronics Program (1985–1999). His current research interests are in the physics and application of ultrasmall structures and novel materials to new high-speed and spin-based electronic and optoelectronic devices and systems. He has supervised over 65 Ph.D. students, and has over 650 publications and 14 issued U.S. patents in these areas.

Dr. Harris is a Fellow of the American Physical Society. He received the 2000 IEEE Morris N. Liebmann Memorial Award, the 2000 International Compound Semiconductor Conference Welker Medal, an IEEE Third Millennium Medal, and an Alexander von Humboldt Senior Research Prize in 1998 for his contributions to GaAs devices and technology.